Measurements of solar energy absorption in a solar collector using carbon nanofluids

Berto, Arianna; Mattiuzzo, Nicolò; Zanetti, Emanuele; Meneghetti, Moreno; Del Col, Davide

DOI
10.1016/j.renene.2024.120763

Publication date
2024

Document Version
Final published version

Published in
Renewable Energy

Citation (APA)
Berto, A., Mattiuzzo, N., Zanetti, E., Meneghetti, M., & Del Col, D. (2024). Measurements of solar energy absorption in a solar collector using carbon nanofluids. *Renewable Energy*, *230*, Article 120763. https://doi.org/10.1016/j.renene.2024.120763

Renewable Energy 230 (2024) 120763

Contents lists available at ScienceDirect

Renewable Energy

journal homepage: www.elsevier.com/locate/renene

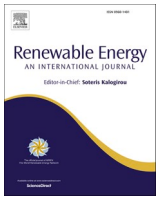

Measurements of solar energy absorption in a solar collector using carbon nanofluids

Arianna Berto [a], Nicolò Mattiuzzo [a], Emanuele Zanetti [a,b], Moreno Meneghetti [c], Davide Del Col [a,*]

[a] Department of Industrial Engineering, University of Padova, Via Venezia 1, 35131, Padova, Italy
[b] Department of Process and Energy, Delft University of Technology, Leeghwaterstraat 39, 2628 CB, Delft, the Netherlands
[c] Department of Chemical Sciences, University of Padova, Via Marzolo 1, 35131, Padova, Italy

ARTICLE INFO

Keywords:
Nanofluids
Carbon nanofluids
Solar collector
DASC
Volumetric solar collector
Thermal efficiency

ABSTRACT

To overcome the limitations of conventional solar thermal collectors (high conductive and convective thermal resistances between the absorber and the fluid), a promising technology is represented by direct absorption solar collectors working with nanofluids, where the incoming solar irradiance is absorbed directly within the volume of fluid. The main issue hindering the diffusion of such technology is related to its reliability, since nanofluids can lose their chemical stability due to nanoparticles sedimentation. Thus, the present work aims at investigating the stability and absorption capability of two nanofluids made of Single-Wall-Carbon-NanoHorns in a volumetric solar receiver.

The present investigation covers the study of material compatibility, the laboratory measurements of nanofluid absorbance and the field simultaneous measurement of thermal and optical efficiency. Since the final performance of direct absorption solar collectors strongly depends on the nanofluid stability, the double efficiency measurement allows to better verify any possible instability effect. Furthermore, field measurements during nanofluid circulation are rare in the literature.

The efficiency of the volumetric solar collector is between 88 % and 92 % at null reduced temperature difference. Finally, tests are performed at high flow rate leading to an evident performance degradation, due to nanoparticles deposition, that can be reversed with sonication.

1. Introduction

Heat is the largest energy end-use, accounting for half of global final energy consumption, significantly more than electricity (20 %) and transport (30 %) [1]. The supply of heat, which contributed more than 40 % to the global related CO_2 emissions in 2020, remains heavily fossil fuel dependent, with renewable sources (including biomass) meeting less than a quarter of global heat demand in 2020. According to the International Energy Agency (IEA), about 46 % of the total thermal power consumed in 2021 was related to space and water heating in buildings. With energy used for heating being significant, heat decarbonization is therefore critical [2].

Over recent years, solar thermal collectors at low and medium temperature (lower than 200 °C) have proved to be a reliable solution to supply heat and decarbonize the thermal needs in residential and industrial sectors [3]. According to the International Renewable Energy Agency (IRENA), at the end of 2020 the total capacity of solar power plants was 1218 GW [4]. Of this amount, 710 GW was electric power generated by solar photovoltaic plants, 7 GW was thermal power produced by solar concentrating systems and 501 GW was thermal power from solar collectors [5]. Therefore, the market around solar thermal collectors is still large, but it is important to improve the existing standard technology and to reduce capital costs.

Conventional flat solar collectors are characterized by the presence of surface-based absorbers, where the solar radiation is firstly converted into heat and then transferred to a working fluid by thermal conduction and convection. The main disadvantage of this system is the overheating of the receiver surface, which enhances the thermal losses towards the environment and leads to a decrease in the thermal efficiency. This drawback can be addressed by allowing the incident solar radiation to directly interact with the heat transfer fluid, without heating any other component in the receiver.

* Corresponding author.
E-mail address: davide.delcol@unipd.it (D. Del Col).

https://doi.org/10.1016/j.renene.2024.120763
Received 7 December 2023; Received in revised form 27 May 2024; Accepted 3 June 2024
Available online 3 June 2024

In direct absorption solar collectors (DASCs) the conversion of solar energy into heat occurs directly within the volume of fluid which acts as the absorber [6]. This solution allows to improve the thermal efficiency of the system and to reduce the costs and the collector environmental impact due to the absence of the selective absorber surface (which represents the main cost item in solar collectors). Compared to conventional solar collectors, a significant environmental benefit of DASCs relies on the smaller energy consumption during manufacturing, since large part of the solar collector materials is replaced by stainless steel and glass instead of copper [7]. Otanicar and Golden [8] estimated that, with reference to a 3-person family dwelling using 188 L of hot water daily from a mix of electric and natural gas water heaters, DASCs would allow to save 34 kg of CO_2 equivalent emissions during the manufacturing process.

Due to the advances in the field of nanotechnologies, growing interest has been addressed to the potential use of the so-called nanofluids inside DASCs due to their favourable thermophysical and optical properties [9–11]. Nanofluids can be suitably employed as heat transfer vectors in DASCs due to the low risk of mechanical or chemical erosion, fouling of hydraulic loops or clogging of pumps compared to microparticle-based fluids.

The key challenge still hindering the widespread employment of nanofluids is related to their chemical stability, since destabilization factors (such as high temperatures, intense solar radiation, thermal/solar cycles, …) may induce the nanoparticles collision and, therefore, their clustering and sedimentation.

Carbon-based nanofluids have raised great interest among researchers due to their excellent chemical stability and broad absorption spectrum characteristics [12]. Moreover, the addition of small concentrations of carbon nanoparticles can greatly enhance the optical properties of the base fluid and improve the efficiency of the solar collector [13,14]. In the work of Sani et al. [15], the stability and the optical characteristics of Single-Wall Carbon NanoHorns (SWCNHs) suspensions in ethylene glycol were studied. High absorbed energy fractions were obtained with SWCNHs samples over short light penetration distances, showing that an efficient sunlight absorption can be obtained with nanofluid volumes smaller than those of usual heat transfer fluids. Li et al. [16] studied the stability and the solar-thermal conversion efficiency of hybrid nanofluids made of silicon carbide and Multi-Wall-Carbon-NanoTubes (MWCNTs), concluding that 0.5 wt% SiC-MWCNTs nanofluids could absorb 99.9 % of the solar energy with only 1 cm path length. The nanofluids displayed an excellent stability during static settlement experiments over one month, while high temperatures and repeated heating cycles were found to influence the nanofluid absorption characteristics.

The synthesis of nanofluids requires advanced and sophisticated equipment, which nevertheless do not necessarily increase the nanofluid's production costs [17]. Indeed, since only a small amount of nanoparticles is added to the base fluid (around 1 %), the final price of the nanofluid is not expected to be significant [18]. Otanicar and Golden [8] carried out an economic and environmental comparison between conventional and nanofluid-based solar collectors for domestic hot water systems. The nanofluid-based solar collector demonstrated higher solar energy conversion efficiency but a slightly longer payback period due to the current market cost for nanoparticles and nanofluid synthesis procedure. Any drop in the price of nanoparticles, which is to be expected as they become more widely employed, would result in further savings for the nanofluid-based solar collector. During 15 years operation of the nanofluid-based solar collector, it could reduce CO_2 emissions to the environment by 740 kg compared to a conventional solar collector and by more than 23000 kg with respect to fossil fuel-based heaters. Moreover, the authors showed that, if nanofluid-based solar collectors were employed by 50 % of the residents of Phoenix (Arizona), over one million tons of CO_2 would be avoided per year.

Most of the experimental works available in the literature on DASCs deal with the investigation of the stability and absorption properties of nanofluids under exposure to a radiative flux in the absence of fluid flow [19,20]. In general, there is a lack of experimental studies focused on the evaluation of the performance of a DASC with flow of carbon nanofluids. Among the few exceptions available in the literature, Delfani et al. [21] experimentally observed that, as the nanoparticles volume fraction and mass flow rate increase, the thermal efficiency of a DASC operating with functionalized MWCNTs in water and ethylene glycol mixture rises with an asymptotic trend. The nanofluids were found to improve the collector efficiency by 10–29 % with respect to the base fluid. Struchalin et al. [22] concluded that exists an optimal mass flow rate (in the range 6–8 L min^{-1}) that maximizes the thermal efficiency of a tubular DASC operating with a MWCNTs-based nanofluid. Indeed, a decrease in the flow rate below the optimal value increases the irradiation time of the particles in the frontal layers of nanofluid and their superheating, leading to higher thermal losses. The same can be inferred in the case of a mass flow rate increase, which would intensify the heat transfer between the wall and the nanofluid and, thus, affect the thermal performance of the solar collector. The thermal efficiency of the tested device was 6–38 % higher compared to an equivalent geometry with surface absorption and the nanofluid demonstrated high stability, remaining homogeneous for at least six months after production. Similarly, Mahbubul et al. [23] tested an evacuated tube solar collector with a SWCNHs nanofluid and obtained an almost linear increasing trend of the thermal efficiency with mass flow rate (600–1000 L h^{-1}). With regard to the effect of the circulation on the stability of the nanofluid, Zanetti et al. [24] observed that nanofluids made of functionalized and oxidized SWCNHs in deionized water were subject to severe degradation after circulation tests at 300 kg h^{-1} in a volumetric solar receiver. Such result was probably due to the interaction between the nanofluid and the moving parts of the pump or to the non-optimal synthesis procedure.

The present paper aims at investigating experimentally the stability and the absorption capability of two carbon nanofluids with different nanoparticles concentration. To cover the existing gap in the literature, field measurements of optical and thermal efficiency of the solar receiver are reported together with the laboratory analysis of the nanofluids absorbance spectra to get information about potential instability issues. Finally, tests are performed at high flow rate to assess the effect of circulation on the DASC performance.

2. Experimental setup

A sketch of the experimental setup is reported in Fig. 1. The experimental setup consists of a primary loop for the nanofluid and an auxiliary water circuit. In the primary loop, an inverter-controlled rotary vane pump is used to circulate the nanofluid exiting the solar receiver.

The nanofluid mass flow rate can be measured by two Coriolis mass flow meters, which are calibrated in two different measuring ranges: 0–90 kg h^{-1} (±0.1 % accuracy at $\dot{m}_n \geq 14$ kg h^{-1}, ±0.27 % otherwise) and 25–400 kg h^{-1} (±0.1 % accuracy). Then, the nanofluid is heated up or cooled down in a tube-in-tube heat exchanger, where water flows in counter-current as secondary fluid in the external annulus. Hot or cold water can be respectively provided by using electrical resistances or a plate heat exchanger releasing heat to the groundwater.

The heat exchanger is 0.5 m long and the inner diameter of the internal tube is equal to 8 mm. After the heat exchanger, the nanofluid is sent back to the solar receiver.

The nanofluid solar receiver is made of two rectangular anti-reflective glass sheets with dimension 500 × 60 × 3 mm, embedded in two stainless steel frames, and three PEEK layers combined to form the channel for the nanofluid passage (depth of 18 mm). This solar receiver has been tested in previous experimental studies ([13,24]). A ball valve is located at the top of the DASC to remove the air trapped inside the loop. The PVC tubes used for connections are thermally insulated and shielded with aluminum tape to limit the convective and radiative thermal losses towards the ambient.

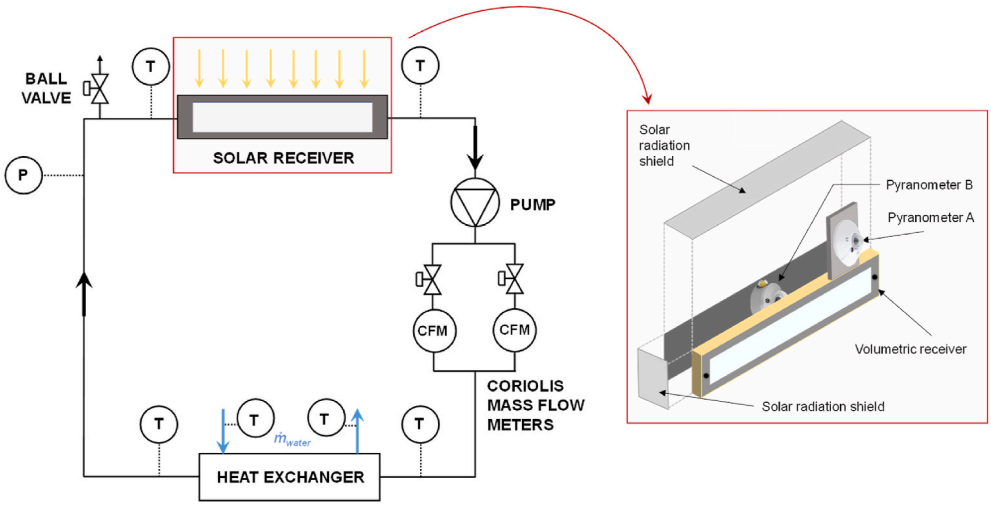

Fig. 1. Sketch of the experimental setup.

The nanofluid loop is mounted on a movable cart which allows to modify the azimuth and the tilt angle of the system and keep the test section perpendicular to the solar rays (the incidence angle is always smaller than 2.5°).

The nanofluid temperatures at the inlet and outlet of both the DASC and the tube-in-tube heat exchanger are measured using four PT-100 type RTDs (±0.03 °C accuracy). Other three PT-100 type RTDs are used to evaluate the inlet and outlet water temperatures in the heat exchanger and the ambient temperature. A pressure transducer is located before the solar receiver to check the nanofluid absolute pressure (±2 mbar).

As shown in Fig. 1, two pyranometers (secondary standard class) are respectively located on the front and on the back of the test section to evaluate the global tilted irradiance (GTI) on two planes parallel to the receiver one. The double-glazing structure of the solar receiver allows the radiation that is not absorbed by the nanofluid to pass through the rear glass. Therefore, the transmitted irradiance GTI_{trans} is measured by the pyranometer positioned on the back (Pyranometer B in Fig. 1), embedded inside a box to be partially shielded from the solar radiation. Instead, the incident solar irradiance onto the collector surface GTI_{inc} is measured by the external pyranometer (Pyranometer A in Fig. 1). Two additional pyranometers are respectively used to evaluate the diffuse horizontal irradiance (DHI) and the global horizontal irradiance (GHI).

Agilent Technologies 34970 A data acquisition unit is used to collect the signals coming from all the sensors every 10 s. Samples of thirty subsequent measurements, corresponding to 5 min of acquisition, are considered for the calculation of the average value of each measured parameter.

3. Characterization of nanofluids and materials compatibility

The nanofluids used for the tests (hereinafter referred to as "Nanofluid1" and "Nanofluid2") consist of suspensions of functionalized SWCNHs (Single-Wall-Carbon-NanoHorns) nanoparticles in deionized water.

The SWCNHs aggregates (about 0.1 g) were first oxidized with a sulphonitric mixture (H_2SO_4:HNO_3 = 3:1 in volume) and then dispersed in the base fluid by means of magnetic stirring, homogenization and sonication (at different power, frequency levels and for different time intervals). The oxidized product was separated and collected by centrifugation. In the second step, the oxidized SWCNHs were functionalized with 750 Da polyethylene glycol chains (PEG-ylation) using a reaction of amidation. Amidation with PEG guarantees a better stability of the SWCNHs suspension and a higher absorption capability compared to oxidized non-PEG-ylated products [24]. The functionalized and oxidized SWCNHs are then diluted with deionized water in order to reach the desired absorption characteristics. More details regarding the preparation procedure of the nanofluids are reported in Ref. [25].

The dilution of Nanofluid1 was calibrated to obtain the optimal absorption efficiency with the minimum expense for the nanofluid preparation. The theoretical absorption efficiency of the nanofluids, also named "absorbed energy fraction" or "optical efficiency", is evaluated with Eq. (1) following the procedure reported in Berto et al. [25]:

$$\eta_{opt,n} = 1 - \tau = 1 - \int f_\lambda \cdot \tau_\lambda \cdot d\lambda \tag{1}$$

In Eq. (1) λ is the wavelength, τ_λ is the spectral transmittance intended as the ratio of the spectral solar irradiance transmitted by the nanofluid $I_{trans,\lambda}$ to the incident spectral solar irradiance $I_{inc,\lambda}$ (Eq. (2)), f_λ is the ratio of the spectral incident solar irradiance $I_{inc,\lambda}$ to the total incident irradiance I_{inc} (Eq. (3)) and τ is the transmitted energy fraction defined by Eq. (4).

$$\tau_\lambda = \frac{I_{trans,\lambda}}{I_{inc,\lambda}} = \frac{1}{10^{A_\lambda}} \tag{2}$$

$$f_\lambda = \frac{I_{inc,\lambda}}{I_{inc}} \tag{3}$$

$$\tau = \int \tau_\lambda \cdot d\lambda \tag{4}$$

In Eq. (2), A_λ is the spectral absorbance of a reference nanofluid, which can be evaluated with a spectrometer using the Lambert Beer law:

$$A_\lambda = L \cdot \varepsilon_\lambda \cdot C \tag{5}$$

where L is the path length, ε_λ is the molar extinction coefficient and C is the nanoparticles concentration in the solution.

The theoretical optical efficiency of the nanofluid $\eta_{opt,n}$ can be calculated with Eq. (1) using the values of I_{inc} and $I_{inc,\lambda}$ retrieved from the reference Air Mass 1.5 spectral distribution of the solar radiation ([26]) and the values of τ_λ obtained from the absorption spectrum of a reference nanofluid. Fig. 2a) reports the absorbed energy fraction against the optical length for four nanofluids showing different absorbance spectra, obtained by halving ($A_{400nm} = 0.1$), equalising ($A_{400nm} = 0.2$), doubling ($A_{400nm} = 0.4$) and triplicating ($A_{400nm} = 0.6$) the absorbance values of the reference nanofluid (Nanofluid1). As highlighted in the figure, the absorbed energy fraction is higher than 90 % for three of the considered nanofluids at 18 mm path length, which is indeed the depth of the direct absorption solar receiver considered in the present work. The nanofluid with $A_{400nm} = 0.2$ (which is also the reference one) ensures good optical

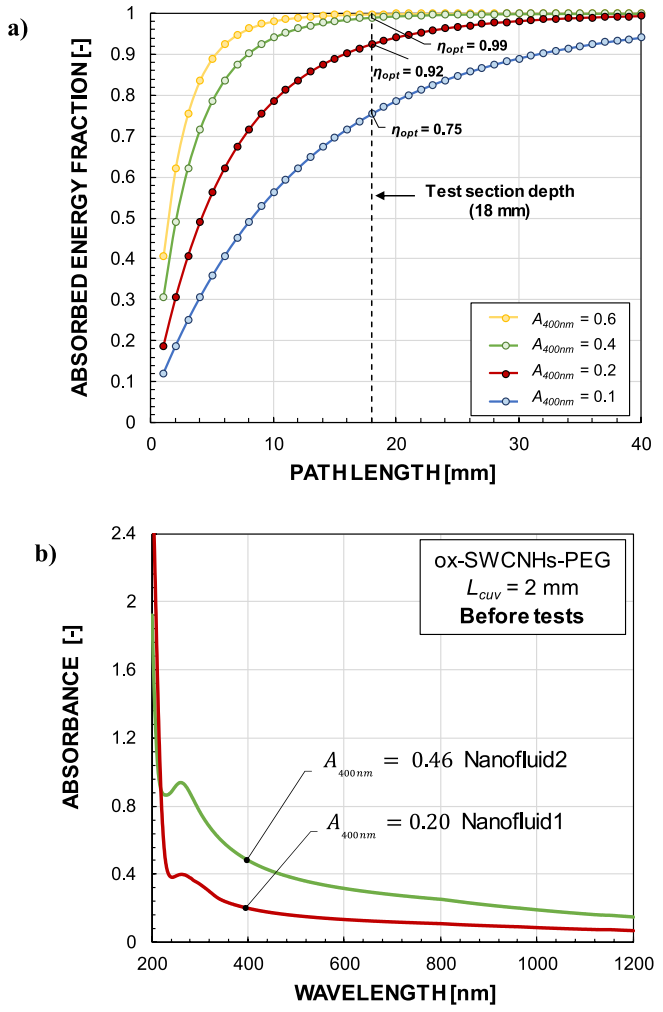

Fig. 2. a) Absorbed energy fraction of four carbon nanofluids with different absorbance spectra as function of the path length (A_{400nm} is the absorbance at λ = 400 nm); b) absorbance spectra of the two SWCNHs nanofluids before starting the experimental campaign.

efficiency at 18 mm path length ($\eta_{opt,n}$ = 0.92), while avoiding further expenditures for increasing the concentration of nanoparticles in the fluid. This nanofluid is here named "Nanofluid1".

The stability and the thermal performance of Nanofluid1 is compared in the present study with those of "Nanofluid2", having A_{400nm} = 0.46 and leading to an optical efficiency equal to 0.99 at 18 mm path length. The final absorbance spectra of the two nanofluids, shown in Fig. 2b), are evaluated with a Cary5000 spectrometer using a 0.2 cm quartz cell. The absorbance spectrum of both nanofluids displays a peak at about 265 nm.

The thermo-physical properties of the tested nanofluids (thermal conductivity and viscosity) were verified to be comparable to those of the base fluid, i.e. water [13].

The compatibility of the nanofluids with different materials was also investigated. Approximately 50 mL of nanofluid with spectral absorbance equal to 2 at 400 nm (using a cuvette with optical path equal to 1 cm) were prepared. The four different materials present in the volumetric solar absorber (i.e. copper, PVC, PEEK, steel) were inserted into separate vials and the nanofluid was then added, taking care that it completely submerged the samples of the aforementioned materials. The whole was left under magnetic stirring continuously for seven days. At the end of this period the solutions with the materials appeared as in Fig. 3a).

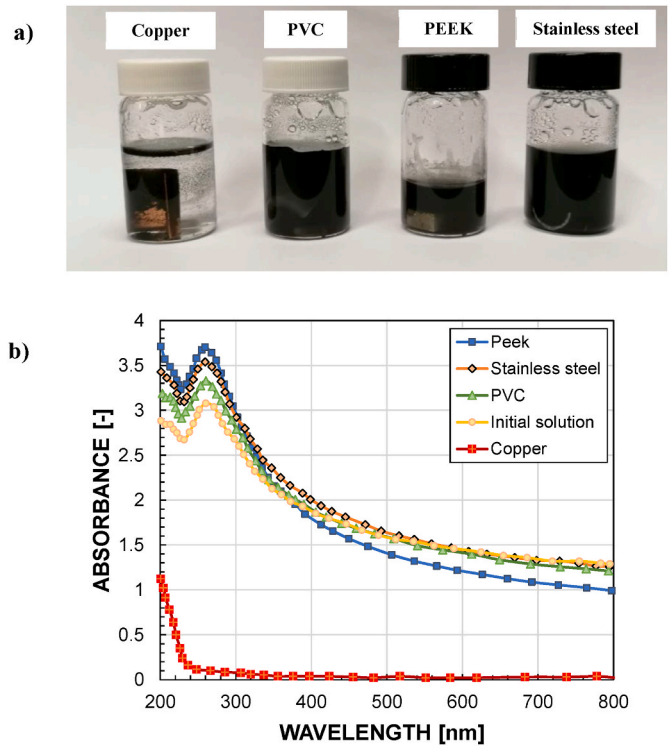

Fig. 3. a) SWCNHs suspensions with materials at the end of the magnetic stirring period; b) absorbance spectra of the nanofluid after being magnetically stirred in the presence of the materials indicated in the legend.

The UV–Vis spectra of the solutions shown in Fig. 3b) were collected by scanning the spectral window 200–800 nm using a quartz cuvette with an optical path of 1 cm. The absorbance of the initial solution, subjected to magnetic stirring, is also reported in Fig. 3b).

From the analysis of the UV–Vis absorption spectra, it can be observed that in the presence of steel, PEEK and PVC the nanofluid shows an improvement in terms of both scattering (which seems to decrease), and maximum absorbance (which increases). This could be due to favourable interactions between the nanoparticles and the materials, or to the continuous agitation of the solution which leads to a better solubilization of the nanomaterials. Instead, the presence of copper promotes the nanofluid degradation, probably due to the contact with synthesis by-products, and therefore its employment in the experimental setup is not recommended. No copper (or brass) components were adopted in the experimental test rig; stainless steel and PVC piping and valves were used instead.

4. Data reduction and uncertainty analysis

The experimental campaign was performed following the guidelines provided by ISO 9806:2017 Standard ([27]) for the identification of steady-state conditions. The aim of the experimental tests is to evaluate the optical and thermal efficiency of the direct absorption solar receiver with the varying operating conditions. According to the Standard ([27]), a collector is considered to operate in steady-state conditions over a given period if none of the experimental parameters deviates from its average value by more than the following limits.

- ±0.1 °C for the nanofluid temperature at the inlet of the solar receiver;
- ±0.4 °C for the nanofluid temperature at the outlet of the solar receiver;
- ±1.5 °C for the air temperature;
- ±50 W m^{-2} for both GTI_{inc} and GTI_{trans} values;

- ±1 % for the nanofluid mass flow rate.

The Standard also imposes a GTI_{inc} minimum value equal to 700 W m^{-2} and an incidence angle of the solar rays on the plane of the receiver smaller than 2.5°. The latter condition was ensured by acting on the movable cart, as discussed in Section 2. Once all the requirements imposed by the Standard are satisfied, the optical efficiency of the receiver is calculated as the ratio of the solar radiation absorbed by the fluid to the incident radiation onto the solar collector aperture area:

$$\eta_{opt,r} = \frac{GTI_{abs}}{GTI_{inc}} \tag{6}$$

where the radiation absorbed by the nanofluid GTI_{abs} is calculated with Eq. (7):

$$GTI_{abs} = GTI_{inc} \cdot \tau_{glass} - \frac{GTI_{trans}}{\tau_{glass}} \tag{7}$$

In Eq. (7) τ_{glass} is the mean transmittance of the glazed area of the receiver (equal to 0.93). If the optical efficiency is referred to the nanofluid, Eq. (6) must be modified as follows:

$$\eta_{opt,n} = \frac{GTI_{abs}}{GTI_{inc} \cdot \tau_{glass}} \tag{8}$$

In Eq. (8) the transmittance of the glass is used to account for the solar irradiance attenuation due to the front glass. The optical efficiency indicated in Eq. (8) can be intended as the absorption capability of the working fluid independently from its enclosure.

It must be noted that since Pyranometer B is located inside a box which is partially shielded from the solar radiation, it displays a reduced field of view compared to Pyranometer A. The two values of irradiance in Eq. (8) are thus referred to different fields of view and cannot be theoretically used in the ratio. To account for this mismatch, the incident solar irradiance must be calculated as follows:

$$GTI_{inc,corr} = DNI + F \cdot DHI \tag{9}$$

In Eq. (9), DNI represents the direct normal irradiance calculated using the Liu and Jordan isotropic model, DHI is the measured diffuse horizontal irradiance and F is a correction factor accounting for the different fields of view of Pyranometers A and B. Since the field of view related to the direct component is the same for both the pyranometers, this correction factor is applied only to the diffuse component of the solar irradiance. The complete analytical and experimental procedure for evaluating the correction factor is provided in Ref. [28].

The thermal efficiency of the solar receiver is computed using Eq. (10):

$$\eta_{th} = \frac{\dot{m}_n \cdot c_n \cdot (T_{out} - T_{in})_n}{GTI_{inc} \cdot A} \tag{10}$$

where $\dot{m}_n$ is the nanofluid mass flow rate, c_n is the nanofluid specific heat, $(T_{out} - T_{in})_n$ is the temperature variation of the nanofluid between inlet and outlet of the solar collector and A is the glazed surface area. The thermal efficiency curve of the receiver is reported against the reduced temperature difference $T_{m,red}$, which is defined as follows (T_{amb} is the ambient temperature):

$$T_{m,red} = \frac{(T_{out} + T_{in})_n / 2 - T_{amb}}{GTI_{inc}} \tag{11}$$

The experimental uncertainty related to the measured parameters is assessed following the JCGM guidelines [29]. The detailed uncertainty procedure is described in the Appendix. The expanded uncertainty (coverage factor $k = 2$) of the optical efficiency is about 12 %, while for the thermal efficiency it ranges from 4 % to 12 %.

All the experimental tests were performed under exposure to non-concentrated solar radiation in Padova, Italy (45° 24′ 23″ N, 11° 52′ 40″ E). Field experiments were divided into two groups: first, tests for evaluating the optical and thermal efficiency of the volumetric solar receiver with the two nanofluids were carried out at small mass flow rate ($\dot{m}_n$ = 5–14 kg h^{-1}) for about 50 h. Then, the effect of circulation on the nanofluids stability was assessed through additional experiments at high mass flow rate ($\dot{m}_n$ = 330 kg h^{-1}) for about 70 h. The absorbance spectra of the nanofluids were checked throughout the two experimental campaigns by means of a spectrometer.

5. Results of efficiency tests (50 hours duration)

Efficiency tests were conducted at nanofluid mass flow rate $\dot{m}_n$ = 5–14 kg h^{-1} and inlet temperature $T_{in,n}$ = 27–50 °C. The mass flow rate was regulated in order to guarantee a temperature difference between inlet and outlet of the solar receiver higher than 1 K. The efficiency values were obtained during about 50 h of tests.

Fig. 4 reports the thermal and optical efficiency of the volumetric solar receiver with both nanofluids against the reduced temperature

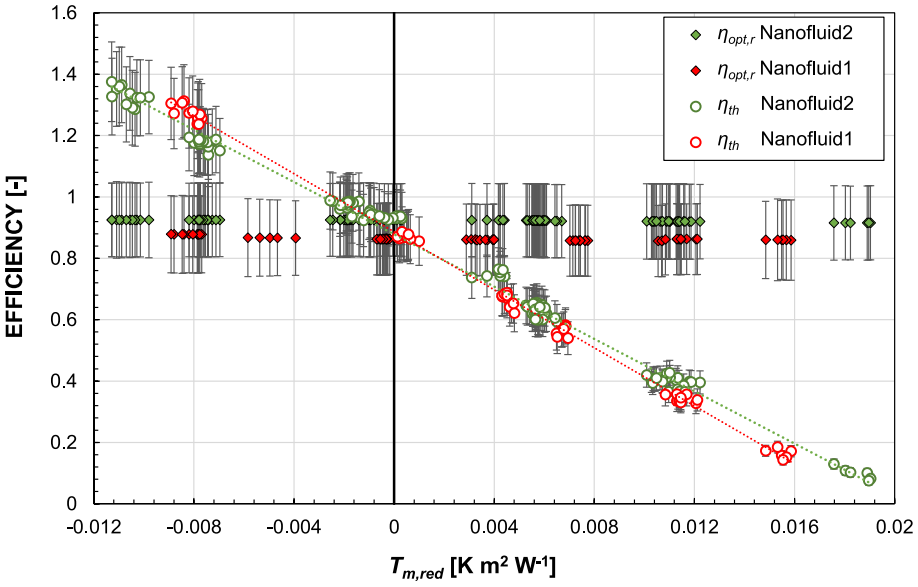

Fig. 4. Optical and thermal efficiency values of the volumetric solar receiver operating with the two SWCNHs nanofluids.

difference. The two nanofluids display similar thermal efficiency curves, while the optical efficiency of the receiver is 7.4 % higher for Nanofluid2 compared to Nanofluid1. The nanofluid optical efficiency, calculated with Eq. (8), is equal to 0.92 and 0.99 for Nanofluid1 and Nanofluid2, respectively, and well agrees with the theoretical one reported in Fig. 2a) at 18 mm path length.

For both nanofluids, at $T_{m,red} = 0$ (i.e. when the mean temperature of the nanofluid at the receiver matches the ambient temperature), the optical and the thermal efficiency values coincide. This result confirms the validity of the newly developed optical technique based on pyranometers.

When the mean temperature of the nanofluids in the receiver is higher than the temperature of the ambient air ($T_{m,red} > 0$), the thermal efficiency is lower than the optical one due to thermal dissipations from the solar receiver to the ambient. On the contrary, when the mean temperature of the nanofluids in the receiver is lower than the ambient temperature ($T_{m,red} < 0$), the thermal efficiency of the solar collector is higher than the optical one due to the heat gain from the ambient.

The slope of the thermal efficiency curves appears to be steeper than conventional plate solar collectors. This behaviour may be related to radiative dissipations occurring through the glazed surface, which is not supplied with any selective coating. Moreover, it is worth underlining that the design of the volumetric receiver was not aimed at maximizing the photo-thermal conversion efficiency, instead it was kept as simple as possible to monitor the stability and the optical behaviour of the nanofluids when used for the direct absorption of the solar radiation. Therefore, there is still margin to increase the values of thermal efficiency of the present DASC, for example by using low-emissivity glass layers or by replacing the glass on the rear side of the receiver with a reflective material and an insulation layer.

The optical efficiency of the solar receiver displays a slightly decreasing trend with the increasing $T_{m,red}$ values. Such reduction, although very little (-3.4 % for Nanofluid1, -2 % for Nanofluid2 in the range of $T_{m,red}$ values from -0.012 to +0.02 K m^2 W^{-1}), may be explained considering that solutions made of PEG can degrade if subjected to several heating cycles owing to the dissociation of water molecules from PEG clustering [25]. This breakup of chemical bonds may alter the absorption capability of the nanofluid.

A sample of few milliliters of nanofluid was collected at the end of each day of test to check if there were changes in the absorbance spectrum during the experimental campaign. Indeed, in case of a reduction in the absorbance values, a degradation of the nanofluid could be inferred due to particles clustering and deposition. In Fig. 5 the absorbance spectra of the two nanofluids at the end of the experimental tests (whose results are reported in Fig. 4) are shown. The absorbance spectra are measured by a Cary5000 spectrometer (Varian) using a 0.2 cm quartz cell.

Comparing Fig. 5 with Fig. 2a), it can be noticed that the absorbance values for both Nanofluids are about 20–30 % lower compared to the initial solution. This result could be explained considering the effect of the working temperature, since its increase can lead to higher collision frequency between nanoparticles, and of subsequent thermal cycles, which can cause breaking of functional groups and change in size/morphology of the nanoparticles [30].

6. Results of circulation tests (70 hours duration)

The stability of the two nanofluids was also assessed at high mass flow rate. Circulation tests under exposure to the solar radiation were conducted at about 330 kg h^{-1}, which allows a transitional flow regime in the receiver [13]. Circulation tests were performed for about 70 h for both fluids.

In Fig. 6, the evolution of the receiver optical efficiency $\eta_{opt,r}$ over time is shown for the two nanofluids and for both efficiency/circulation experiments. Table 1 summarizes the measured $\eta_{opt,r}$ values at the beginning of the tests and after 15, 60 and 70 circulation hours with the two nanofluids. With regard to Nanofluid1, the optical efficiency of the solar receiver was almost stable during efficiency tests, while it shows a slightly decreasing trend during circulation experiments, reaching a final value of 83 % (−1.2 % after 70 h). The same can be argued for Nanofluid2, which instead displays a more marked $\eta_{opt,r}$ reduction during circulation tests (−4.3 % after 70 h).

The analysis of the nanofluid samples collected during the experimental campaign allows to better understand the effect of circulation on the nanofluid stability.

Fig. 7 illustrates the absorbance variations for the two nanofluids during the recirculation tests, detected with Cary5000 spectrometer using a 0.2 cm quartz cuvette. The absorbance slightly decreases over time for Nanofluid1, with a maximum reduction of 16 % after 70 h of circulation. Nanofluid2 shows a much higher decrease in the absorbance value for the same circulation time: after 60 h the nanoparticles concentration is almost close to zero. This faster degradation could be explained considering that the nanofluid clustering frequency is proportional to the square of the density of nanoparticles, and therefore high concentration fluids are more prone to particles collision [30]. Moreover, Sharaf et al. [31] argued that it is unlikely that a stable nanofluid upon standing (whether at ambient conditions or with

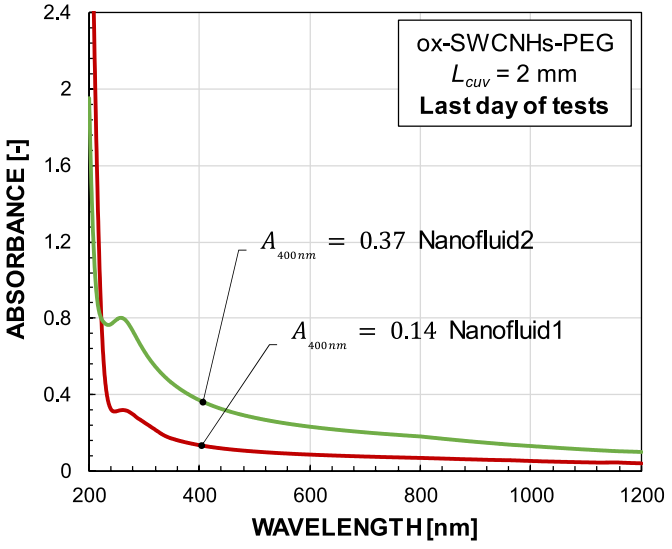

Fig. 5. Absorbance spectra of the two SWCNHs nanofluids after the optical and thermal efficiency experimental tests.

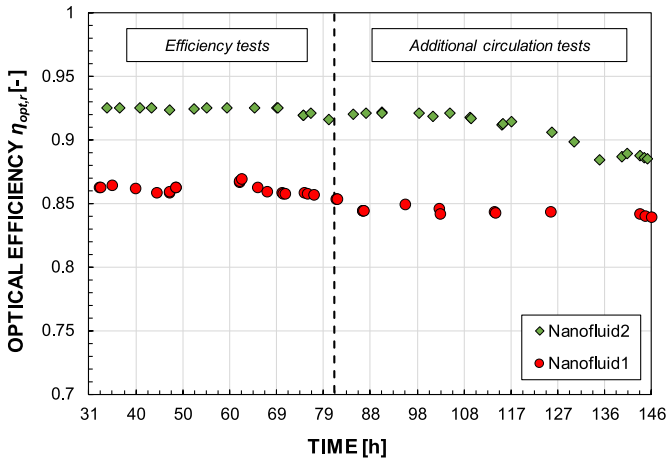

Fig. 6. Optical efficiency of the solar receiver versus time during efficiency tests (50 h) and additional circulation tests (70 h) for the two nanofluids.

Table 1
Comparison between the optical efficiencies of the volumetric solar receiver with the two nanofluids after the same circulation hours.

Circulating hours [h]	$\eta_{opt,r}$ Nanofluid1 [-]	$\eta_{opt,r}$ Nanofluid2 [-]
0	0.85	0.92
15	0.84	0.92
60	0.84	0.88
70	0.84	0.88

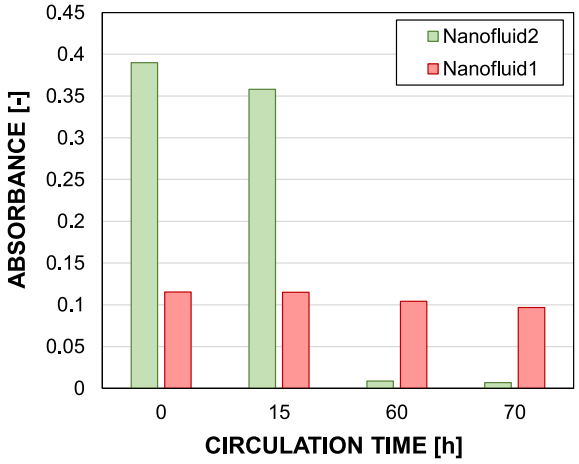

Fig. 7. Absorbance values of the two SWCNHs nanofluids after the same circulation hours (path length of the cuvette equal to 0.2 cm).

exposure to high temperatures/solar radiation) will keep its stability when exposed to shear forces and intense nanoparticles motion. Indeed, nanofluid flow in confined channels can result in lateral migration and deposit of particles close to the channel walls [30].

At the end of the tests, the nanofluids were discharged from the system and it was observed that the internal surface of the rear glass was covered by a black deposit, which was much thicker in the case of Nanofluid2. It is clear that the presence of such deposit may alter the absorption of the solar radiation, resembling the behaviour of a flat solar collector, and impair the reliability of the in-situ measurements.

To better investigate the effect of the black deposit on the experimental data, the solar collector operating with Nanofluid2 was exposed to the solar radiation with and without nanofluid inside. The receiver optical efficiency measured in the two cases is reported in Table 2. The optical efficiency of the DASC was respectively equal to 0.88 and 0.75 considering the cases with nanofluid and without nanofluid. The similar $\eta_{opt,r}$ values confirm the dominant contribution of the rear black deposit on the measured optical efficiency for Nanofluid2.

A comparable investigation was performed also for Nanofluid1. Indeed, two experiments were performed by exposing the DASC with and without rear black deposit to the solar radiation, to evaluate the corresponding optical efficiency of the nanofluid (Table 3). If considering a clean rear glass, a value of $\eta_{opt,n}$ equal to 0.78 was obtained, being close to the nanofluid optical efficiency obtained with the rear black deposit (equal to 0.89). Therefore, the contribution of the black deposit on the optical efficiency of Nanofluid1 was not as significant as for Nanofluid2.

Table 2
Effect of the black nanoparticles deposit on the optical efficiency of the receiver operating with Nanofluid2.

	Case 1 - DASC with black deposit, nanofluid inside	Case 2 - DASC with black deposit, no nanofluid inside
$\eta_{opt,r}$ [−]	0.88	0.75

Table 3
Effect of the black nanoparticles deposit on the optical efficiency of Nanofluid1.

	Case 1 - DASC with black deposit, nanofluid inside	Case 2 - DASC without black deposit, nanofluid inside
$\eta_{opt,n}$ [−]	0.89	0.78

An attempt was made to put the nanoparticles back into suspension through a sonication process in order to get the absorbance spectrum of the initial solution. A sample of nanoparticles was taken from the black deposit on the rear glass of the receiver (shown in Fig. 8) and sonicated for about 1 h.

Fig. 8 shows the absorbance spectra of the initial solution, of the nanofluid after 70 h of circulation and after sonication, evaluated using Cary5000 spectrometer (0.2 cm quartz cuvette). Thanks to sonication, the nanoparticles are completely back in suspension and the shape of the resulting absorbance spectrum, as well as its values, resemble the original one.

This result suggests that the presence of a sonicator in the experimental setup would be favourable for keeping the nanofluid under agitation even during periods of plant inactivity and for bringing any deposited particles back into suspension.

7. Conclusions

Direct absorption solar collectors (DASCs) represent a promising technology for decarbonizing the thermal needs in residential and industrial sectors and increasing the thermal efficiency compared to flat plate solar collectors. However, the reliability of this technology mainly depends on the stability of the nanofluids employed as working fluids, which may experience clustering/sedimentation of nanoparticles.

In the present work, the stability and the absorption capability of two nanofluids (namely “Nanofluid1” and “Nanofluid2”), obtained from Single Wall Carbon Nanohorns (SWCNHs) and having different nanoparticles concentration, was experimentally assessed within a DASC. The nanoparticles concentration of Nanofluid2 was more than two times higher compared to Nanofluid1. The present investigation covers the study of material compatibility for the tested nanofluids, the laboratory measurements of nanofluid absorbance and the field simultaneous measurement of thermal and optical efficiency.

The main outcomes are the followings:

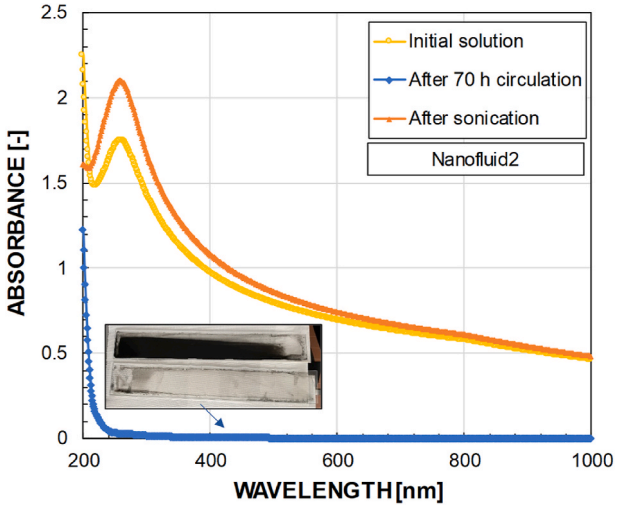

Fig. 8. Absorbance spectra of Nanofluid2 at the beginning of the experimental tests, after 70 h of circulation and after sonication (path length of the cuvette equal to 0.2 cm). An image of the black deposit on the rear side of the solar receiver is also shown.

- The interaction between copper and carbon nanofluids leads to a fast nanoparticles agglomeration, therefore the employment of other more compatible materials (such as steel and PVC) in the experimental setup is highly recommended.
- The receiver thermal and optical efficiency values coincide at null reduced temperature difference and range between 88 % and 92 %. The thermal efficiency curve displays a linear trend but a steeper slope compared to conventional plate solar collectors due to the higher convective/radiative thermal losses through the glazed surface and to the non-optimized collector geometry.
- After about 70 h of circulation at high flow rate (equal to 330 kg h^{-1}), the nanoparticles concentration for Nanofluid2 was nearly zero, while the absorbance values of Nanofluid1 showed a much smaller decrease over time. This faster degradation could be explained considering that high concentration fluids are more prone to nanoparticles collision and agglomeration.
- A deposit of nanoparticles on the rear glass of the receiver was observed for both Nanofluid1 and Nanofluid2, although for the latter the deposit layer was much thicker. However, it was possible to restore the initial absorption spectrum of the nanofluid through sonication of deposited nanoparticles.

To conclude, the reduction of nanoparticles concentration, together with the development of new synthesis procedures and the adoption of specific devices (such as sonicators for the continuous dispersion of nanoparticles), can potentially increase the nanofluids long-term reliability in field deployment. Moreover, the design of the DASC must be approached by properly selecting the fabricating materials, which must be compatible with nanofluids, and by optimizing the geometry to maximize the thermal efficiency.

Data availability

Reported data can be made available to the reader upon request to the authors.

CRediT authorship contribution statement

Arianna Berto: Conceptualization, Data curation, Formal analysis, Investigation, Validation, Visualization, Writing – original draft, Writing – review & editing. **Nicolò Mattiuzzo:** Data curation, Formal analysis, Investigation, Visualization. **Emanuele Zanetti:** Conceptualization, Methodology, Writing – original draft, Writing – review & editing. **Moreno Meneghetti:** Conceptualization, Methodology, Resources, Supervision, Writing – original draft, Writing – review & editing. **Davide Del Col:** Conceptualization, Funding acquisition, Methodology, Project administration, Resources, Supervision, Writing – review & editing.

Declaration of competing interest

The authors declare the following financial interests/personal relationships which may be considered as potential competing interests:

Davide Del Col reports financial support was provided by Ministero Italiano Universita' e Ricerca - Unione Europea. If there are other authors, they declare that they have no known competing financial interests or personal relationships that could have appeared to influence the work reported in this paper.

Acknowledgments

This research study was developed in the framework of the research activities carried out within the Project "Network 4 Energy Sustainable Transition—NEST", Spoke 1, Project code PE0000021, funded under the National Recovery and Resilience Plan (NRRP), Mission 4, Component 2, Investment 1.3 - Call for tender No. 1561 of 11.10.2022 of Ministero dell'Università e della Ricerca (MUR); funded by the European Union—NextGenerationEU.

Giovanni Ponzana and Sebastiano Pasinato from the Department of Chemical Sciences of the University of Padova are greatly acknowledged for preparing the two nanofluids.

Mario Junio Gabellone and Giacomo Marrocu from the Department of Industrial Engineering of the University of Padova are greatly acknowledged for their help during the experimental campaigns.

The present paper is an extended version of a work presented at the 18th Conference on Sustainable Development of Energy, Water and Environment Systems (SDEWES), held from 24 to September 29, 2023 in Dubrovnik (Croatia).

NOMENCLATURE

A	Absorbance
C	Concentration of nanoparticles in the solution, g L^{-1}
c	Heat capacity, J kg^{-1} K^{-1}
DHI	Diffuse solar irradiance on a horizontal surface, W m^{-2}
DNI	Direct normal irradiance, W m^{-2}
f_λ	Fraction of the total incident solar irradiance GTI_{inc} at specific wavelength, $f_\lambda = GTI_{inc,\lambda}/GTI_{inc}$ F Correction factor for the diffuse component of the solar irradiance
GHI	Global irradiance on a horizontal surface, W m^{-2}
GTI	Global tilted irradiance, W m^{-2}
I	Irradiance, W m^{-2}
k	Coverage factor
L	Path length, mm
$\dot{m}$	Mass flow rate, kg s^{-1}
N	Number of sample points
T	Temperature, K
u	Standard uncertainty
U	Expanded uncertainty

Greek symbols

η_{opt}	Optical efficiency
η_{th}	Thermal efficiency
τ	Transmittance

ε_λ	Molar extinction coefficient, L mm^{-1} g^{-1}
σ	Standard deviation
λ	Wavelength, nm

Subscripts

λ	Spectral
abs	Absorbed
amb	Ambient
corr	Corrected
cuv	Cuvette
glass	Glass layer
in	Inlet
inc	Incident
n	Nanofluid
out	Outlet
r	Receiver
trans	Transmitted

Abbreviations

DASC	Direct Absorption Solar Collector
MWCNT	Multi Wall Carbon NanoTubes
PEG	Polyethylene Glycol
SWCNH	Single Wall Carbon NanoHorn

Appendix

The experimental uncertainty on the reported data is assessed following the JCGM guidelines [29]. The standard combined uncertainty of the measured parameters is evaluated with the following equation:

$$u = \sqrt{u_A^2 + u_B^2} \tag{A.1}$$

where the Type A uncertainty u_A is associated to the standard deviation of the sample and the Type B uncertainty u_B is obtained from manufacturers' specifications and calibration certificates. Since the size of the sample of experimental data is small, the Student's t-distribution is applied to evaluate the Type A uncertainty as indicated in Eq. (A.2):

$$u_A = \frac{\sigma}{\sqrt{N}} \cdot t_{STUD} \tag{A.2}$$

where σ is the standard deviation of the 30 values used to calculate the average of each measured parameter, N is the number of data points (equal to 30 in this case) and t_{STUD} refers to the Student's t-distribution values, with (N-1) degrees of freedom.

The Type B uncertainties of the employed sensors are listed in Table A1. With regard to pyranometers, several Type B uncertainty contributions must be taken into account, as reported in Table A2.

The standard uncertainty calculated with Eq. (A.1) is multiplied by the coverage factor k to evaluate the expanded uncertainty U, as shown in Eq. (A.3). In order to have a confidence value of 95.4 %, the coverage factor is fixed as 2.

$$U = k \cdot u \tag{A.3}$$

The law of uncertainty propagation is employed to calculate the standard uncertainty of non-directly measured parameters, such as the optical and the thermal efficiency values. Indeed, if y is the unknown parameter calculated as function of x_1, x_2, …, x_Z measured variables, the law of uncertainty propagation can be applied as follows:

$$u_y = \sqrt{\sum_{i=1}^{Z} \left(\frac{\partial y}{\partial x_i}\right)^2 \cdot u_{x_i}^2} = \sqrt{\left(\frac{\partial y}{\partial x_1}\right)^2 \cdot u_{x_1}^2 + \left(\frac{\partial y}{\partial x_2}\right)^2 \cdot u_{x_2}^2 + \ldots + \left(\frac{\partial y}{\partial x_Z}\right)^2 \cdot u_{x_Z}^2} \tag{A.4}$$

The expanded uncertainty of the optical efficiency is generally constant and on average equal to 12 %, while for the thermal efficiency it ranges from 4 % to 12 %. With regard to the reduced temperature difference, the related expanded uncertainty varies between ±0.0009 K m^2 W^{-1} and ±0.0015 K m^2 W^{-1}.

Table A.1
Type B experimental uncertainty of measured parameters (95 % confidence).

Temperature	±0.03 °C
Pressure	±0.05 % full scale (4 bar)
Nanofluid mass flow rate (CFM_1 0–90 kg h^{-1})	±0.1 % of the reading at $\dot{m}_n \geq 14$ kg h^{-1} ±0.27 % of the reading at $\dot{m}_n = 5$ kg h^{-1}
Nanofluid mass flow rate (CFM_2 25–400 kg h^{-1})	±0.1 % of the reading

Table A.2
Type B uncertainty contributions of the employed pyranometers.

Uncertainty source	*Zipp and Zonen CM11 (GTI_{inc} and GTI_{trans})*	*Zipp and Zonen CMP22 (DHI)*	*DeltaOHM LP PYRA (GHI)*
Calibration	±1.5 % of the reading		
Non-stability	±0.5 % of the reading per year		±1.5 % of the reading per year
Non-linearity	±0.6 % of the reading	±0.2 % of the reading	±1 % of the reading
Zero-offset A	±12 W m^{-2}	±3 W m^{-2}	±4 W m^{-2}
Zero-offset B	±7 W m^{-2}	±1 W m^{-2}	±15 W m^{-2}
Temperature response	±1 % of the reading	±0.5 % of the reading	±4 % of the reading
Spectral response	±2 % of the reading		±5 % of the reading
Tilt response	±0.2 % of the reading		
Direction response	±0.5 % of the reading		–

References

[1] International Energy Agency (IEA), Renewables 2020 - Analysis and Forecast to 2025, 2020.
[2] P.A. Østergaard, N. Duic, Y. Noorollahi, S. Kalogirou, Renewable energy for sustainable development, Renew. Energy 199 (2022) 1145–1152, https://doi.org/10.1016/j.renene.2022.09.065.
[3] P.A. Østergaard, N. Duic, Y. Noorollahi, S. Kalogirou, Advances in renewable energy for sustainable development, Renew. Energy 219 (2023), https://doi.org/10.1016/j.renene.2023.119377.
[4] International Renewable Energy Agency (IRENA), Renewable Capacity Statistics 2021, 2021.
[5] M. Weiss, Werner and Spörk-Dür, Solar Heat Worldwide – Global Market Development and Trends in 2020-Detailed Market Data 2019, 2021 Edition, 2021.
[6] M. Sainz-Mañas, F. Bataille, C. Caliot, A. Vossier, G. Flamant, Direct absorption nanofluid-based solar collectors for low and medium temperatures, A review, Energy 260 (2022), https://doi.org/10.1016/j.energy.2022.124916.
[7] Z. Said, A.A. Hachicha, S. Aberoumand, B.A.A. Yousef, E.T. Sayed, E. Bellos, Recent advances on nanofluids for low to medium temperature solar collectors: energy, exergy, economic analysis and environmental impact, Prog. Energy Combust. Sci. 84 (2021), https://doi.org/10.1016/j.pecs.2020.100898.
[8] T.P. Otanicar, J.S. Golden, Comparative environmental and economic analysis of conventional and nanofluid solar hot water technologies, Environ. Sci. Technol. 43 (2009) 6082–6087, https://doi.org/10.1021/es900031j.
[9] T.B. Gorji, A.A. Ranjbar, S.N. Mirzababaei, Optical properties of carboxyl functionalized carbon nanotube aqueous nanofluids as direct solar thermal energy absorbers, Sol. Energy 119 (2015) 332–342, https://doi.org/10.1016/j.solener.2015.07.012.
[10] A. Moradi, E. Sani, M. Simonetti, F. Francini, E. Chiavazzo, P. Asinari, Carbon-nanohorn based nanofluids for a direct absorption solar collector for civil application, J. Nanosci. Nanotechnol. 15 (2015) 3488–3495, https://doi.org/10.1166/jnn.2015.9837.
[11] E.P. Bandarra Filho, O.S.H. Mendoza, C.L.L. Beicker, A. Menezes, D. Wen, Experimental investigation of a silver nanoparticle-based direct absorption solar thermal system, Energy Convers. Manag. 84 (2014) 261–267, https://doi.org/10.1016/j.enconman.2014.04.009.
[12] P. Raj, S. Subudhi, A review of studies using nanofluids in flat-plate and direct absorption solar collectors, Renew. Sustain. Energy Rev. 84 (2018) 54–74, https://doi.org/10.1016/j.rser.2017.10.012.
[13] M. Bortolato, S. Dugaria, F. Agresti, S. Barison, L. Fedele, E. Sani, D. Del Col, Investigation of a single wall carbon nanohorn-based nanofluid in a full-scale direct absorption parabolic trough solar collector, Energy Convers. Manag. 150 (2017) 693–703, https://doi.org/10.1016/j.enconman.2017.08.044.
[14] S. Dugaria, M. Bortolato, D. Del Col, Modelling of a direct absorption solar receiver using carbon based nanofluids under concentrated solar radiation, Renew. Energy 128 (2018) 495–508, https://doi.org/10.1016/j.renene.2017.06.029.
[15] E. Sani, L. Mercatelli, S. Barison, C. Pagura, F. Agresti, L. Colla, P. Sansoni, Potential of carbon nanohorn-based suspensions for solar thermal collectors, Sol. Energy Mater. Sol. Cells 95 (2011) 2994–3000, https://doi.org/10.1016/j.solmat.2011.06.011.
[16] X. Li, G. Zeng, X. Lei, The stability, optical properties and solar-thermal conversion performance of SiC-MWCNTs hybrid nanofluids for the direct absorption solar collector (DASC) application, Sol. Energy Mater. Sol. Cells 206 (2020) 110323, https://doi.org/10.1016/j.solmat.2019.110323.
[17] M.S. Bretado-de los Rios, C.I. Rivera-Solorio, K.D.P. Nigam, An overview of sustainability of heat exchangers and solar thermal applications with nanofluids: a review, Renew. Sustain. Energy Rev. 142 (2021) 110855, https://doi.org/10.1016/j.rser.2021.110855.
[18] F.S. Javadi, R. Saidur, M. Kamalisarvestani, Investigating performance improvement of solar collectors by using nanofluids, Renew. Sustain. Energy Rev. 28 (2013) 232–245, https://doi.org/10.1016/j.rser.2013.06.053.
[19] T.B. Gorji, A.A. Ranjbar, A review on optical properties and application of nanofluids in direct absorption solar collectors (DASCs), Renew. Sustain. Energy Rev. 72 (2017) 10–32, https://doi.org/10.1016/j.rser.2017.01.015.
[20] V. Khullar, V. Bhalla, H. Tyagi, Potential heat transfer fluids (Nanofluids) for direct volumetric absorption-based solar thermal systems, J. Therm. Sci. Eng. Appl. 10 (2018) 1–13, https://doi.org/10.1115/1.4036795.
[21] S. Delfani, M. Karami, M.A. Akhavan-Behabadi, Performance characteristics of a residential-type direct absorption solar collector using MWCNT nanofluid, Renew. Energy 87 (2016) 754–764, https://doi.org/10.1016/j.renene.2015.11.004.
[22] P.G. Struchalin, V.S. Yunin, K.V. Kutsenko, O.V. Nikolaev, A.A. Vologzhannikova, M.P. Shevelyova, O.S. Gorbacheva, B.V. Balakin, Performance of a tubular direct absorption solar collector with a carbon-based nanofluid, Int. J. Heat Mass Tran. 179 (2021) 121717, https://doi.org/10.1016/j.ijheatmasstransfer.2021.121717.
[23] I.M. Mahbubul, M.M.A. Khan, N.I. Ibrahim, H.M. Ali, F.A. Al-Sulaiman, R. Saidur, Carbon nanotube nanofluid in enhancing the efficiency of evacuated tube solar collector, Renew. Energy 121 (2018) 36–44, https://doi.org/10.1016/j.renene.2018.01.006.
[24] E. Zanetti, S. Dugaria, F. Biscaglia, F. Agresti, L. Fedele, M. Meneghetti, D. Del Col, Investigation of nanofluids circulating in a volumetric solar receiver, J. Therm. Sci. Eng. Appl. 13 (2021) 1–12, https://doi.org/10.1115/1.4049041.
[25] A. Berto, E. Zanetti, G. Ponzana, M. Meneghetti, D. Del Col, In-line measurement of absorbed solar irradiance using a volumetric collector with SWCNH nanofluid, Heat Mass Transf. Und Stoffuebertragung (2022), https://doi.org/10.1007/s00231-022-03271-6.
[26] ASTM G173-03, Reference spectra (reference air mass 1.5 spectra). https://www.nrel.gov/grid/solar-resource/spectra-am1.5.html, 2017. (Accessed 17 February 2022).
[27] ISO, ISO 9806:2017 standard. Solar Energy - Solar Thermal Collectors - Test Methods, 2017.
[28] E. Zanetti, A. Berto, M. Meneghetti, D. Del Col, In-line measurement of absorbed solar irradiance using nanofluids, J. Phys. Conf. Ser. 2116 (1) (2021) 1–4.
[29] Joint Committee for Guides in Metrology (JCGM), Evaluation of measurement data - guide to the expression of uncertainty in measurement, Bur. Int. Des Poids Mes. (BIPM), Sèvres, France (2008). http://www.bipm.org/en/publications/guides/gum.html. (Accessed 29 October 2019).
[30] O.Z. Sharaf, R.A. Taylor, E. Abu-Nada, On the colloidal and chemical stability of solar nanofluids: from nanoscale interactions to recent advances, Phys. Rep. 867 (2020) 1–84, https://doi.org/10.1016/j.physrep.2020.04.005.
[31] O.Z. Sharaf, A.N. Al-Khateeb, D.C. Kyritsis, E. Abu-Nada, Four-way coupling of particle-wall and colloidal particle-particle interactions in direct absorption solar collectors, Energy Convers. Manag. 195 (2019) 7–20, https://doi.org/10.1016/j.enconman.2019.04.069.